

Enhanced mass transport in ultra-rapidly-heated Ni/Si thin-film multilayers

L. P. Cook,^{a,b} R. E. Cavicchi,^a N. Bassim,^{a,c} S. Eustis,^{a,d} W. Wong-Ng,^a I. Levin,^a U. R. Kattner,^a C. E. Campbell,^a C. B. Montgomery,^a W. F. Egelhoff,^a and M. D. Vaudin^a

^aNational Institute of Standards and Technology, Gaithersburg, Maryland 20899

^bPresent address: PhazePro Technologies, LLC, Hustontown, Pennsylvania 17229

^cPresent address: Naval Research Laboratory, Washington, D. C. 20375

^dPresent address: Directed Vapor Technologies International, Inc., Charlottesville, Virginia 22903

(Received

ABSTRACT

We have investigated multilayer and bilayer Ni/Si thin films by nano-differential scanning calorimetry (DSC) at ultra-rapid scan rates, in a temperature-time regime not accessible with conventional apparatus. DSC experiments were completed at slower scan rates as well, where it was possible to conduct parallel rapid thermal annealing (RTA) experiments for comparison. Post-experimental characterization was accomplished by x-ray diffraction (XRD), and by transmission electron microscopy (TEM) and energy- filtered transmission electron microscopy (EFTEM) of thin cross sections prepared by focused ion beam (FIB) milling. We found that rate of heating has a profound effect on the resulting microstructure, as well as on the DSC signal. After heating to 560 °C at 120 °C/s, the general microstructure of the multilayer was preserved, in spite of extensive interdiffusion of Ni and Si. By contrast, after heating to 560 °C at 16,000 °C/s, the multilayer films were completely homogeneous with no evidence of the original multilayer microstructure. For the slower scan rates, we interpret the results as indicating a solid state diffusion-nucleation-growth process. At the higher scan rates, we suggest that the temperature increased so rapidly that a metastable liquid was first formed, resulting in complete intermixing of the multilayer, followed by crystallization to form solid phases. The integrated DSC enthalpies for both multilayer and bilayer films are consistent with this interpretation,

which is further supported by thermodynamic predictions of metastable Ni/Si melting and solid state Ni/Si interdiffusion. Our results suggest that use of heating rates $>10,000$ °C/s may open new avenues for intermetallic micro- and nano-fabrication, at temperatures well below those prevailing during explosive silicidation.

PACS numbers: 64.60.My, 64.70.kg, 64.75.-g, 66.10.cg, 66.30.Ng, 81.30.-t

I. INTRODUCTION

As the technology for complementary metal oxide-semiconductor (CMOS) devices advances to feature sizes of 45 nm and below, replacement of the polysilicon/SiO₂ gate stack combination represents a key paradigm shift. The industry is moving towards a metal gate/high- κ dielectric combination in which fully silicided (FUSI) metal gates are receiving a lot of attention as candidates for the metal layer.¹⁻⁶ An important example is the Ni-Si system which consists of a number of phases with optimal electrical conductivity and work function.² In developing this technology, the thermal stability, and thermal compatibility with other CMOS processes are important factors.¹ The use of ultra-rapid thermal annealing processes which occur on the millisecond time scale are being investigated for the control of dopant distributions in ultra-shallow junctions.^{7,8} It has also recently been demonstrated that the Ni-Si reaction can occur using laser annealing^{9,10} and such ultra-fast processing of Ni-Si represents an important avenue for continuing the Moore's law progression.¹¹ While it seems clear that the processes of diffusion and reaction that are responsible for forming the silicides will have different kinetics, the effect of ramp rate on the reactions remains unexplored.

The Ni-Si reaction has been previously studied with Ni deposited on single crystal Si,⁵ polysilicon,⁶ and for co-sputtered Ni and Si.⁴ During reaction, more than one phase may be present, for example, in the work of Rivero et al,⁵ the reaction proceeded via a mixture of Ni₂Si and Ni₃Si₂ for a 13 nm Ni patch deposited on a single crystal. In experiments with Ni on polysilicon,⁶ it was found that the ratio of the thicknesses of deposited Ni and Si determined the composition of the silicide, with intermediate silicides of NiSi and Ni₃₁Si₁₂ formed during the anneal. Co-sputtering the two materials also allowed control of composition and was shown to affect the work function.⁴ Calorimetric measurements have proven useful at elucidating the processes during a Ni-Si reaction,¹² as have detailed kinetic studies.¹³

It was the aim of this study to explore the Ni-Si reaction at rapid heating rates using a combinatorial approach with a microelectromechanical (MEMS) device that allowed for simultaneous heating and DSC measurements. By comparing post-reaction characterization results for a bilayer with a multilayer of Ni-Si, each with the same total thickness, we were able to investigate the role of interdiffusion. As expected, the reaction was enhanced in the multilayer sample due to a short diffusion distance. The

surprising finding is that there is a strong enhancement of Ni/Si mixing with rapid ramp rate.

II. EXPERIMENTAL PROCEDURE

The nanocalorimeter shown in Figure 1 acts like a miniature differential scanning calorimeter.¹⁴ The device consists of a $66\ \mu\text{m} \times 240\ \mu\text{m} \times 3.3\ \mu\text{m}$ thick inner suspended platform divided into sample and reference zones. The device was fabricated in an array of six elements. Films are deposited on the sample side using a shadow mask. Each zone has an integral poly-Si heater and an Al/poly-Si thermopile for measuring the temperature difference between the two zones. To enhance the thermal isolation of the inner platform, the leads to the thermopile and heater run along a suspended platform that surrounds the inner platform. Chips are mounted in packages and placed in a high vacuum system for calorimetry scans. The thermopile produces a signal of $1.8\ \text{mV/K}$ that yields $1\ \text{mK}$ resolution at a $10\ \text{kHz}$ bandwidth. During a scan, separate heater voltage (V_h) ramps were applied to the sample and reference heaters, and the thermopile signal was recorded using a preamplifier and digital oscilloscope. A set of devices coated with melting point standards (In, Sn, Pb, Al-Ge eutectic) was produced to calibrate temperature and enthalpy for each of the ramp rates used in the Ni-Si measurements. DSC scans consisted of a ramp up to a maximum temperature, followed immediately by a ramp down to room temperature. This sequence was repeated until there was no change in the signal from one scan to the next. The signal from the last scan (which was due to differences in the heat capacity of the reacted sample and the reference side) was used as a baseline which was subtracted from the earlier scans, to provide difference scans showing the progression of the Ni/Si reaction.

Films of Si and Ni were deposited on the nanocalorimeters by magnetron sputtering at a base pressure of $2.7 \times 10^{-6}\ \text{Pa}$. Two sets of samples were prepared with the total Ni and Si content the same for the two sets. Bilayer samples consisted of layers of $100\ \text{nm}$ Ni and $100\ \text{nm}$ Si, and the multilayer films were composed of ten sequences of ($10\ \text{nm}$ Ni/ $10\ \text{nm}$ Si). Films on test coupons of Si wafers coated with $500\ \text{nm}$ of thermal oxide were prepared simultaneously for use in parallel RTA experiments. Post-experimental characterization utilized x-ray diffraction (XRD), focused ion-beam milling and transmission electron microscopy (FIB/TEM), scanning electron microscopy with energy dispersive x-ray analysis (SEM/EDS), and reflected light microscopy.

Samples for TEM from individual devices were cut and thinned using FIB methods. Compositional mapping was accomplished using energy-filtered TEM (EFTEM) in a JEOL 3010 UHR TEM ($300\ \text{kV}$) equipped with a Gatan Imaging Filter. The Si $L_{2,3}$ edge, Ni $M_{2,3}$ and Ni $L_{2,3}$ absorption edges were used¹⁵. A three-window method was used to isolate the signal from the background. Partial overlap of the Ni $M_{2,3}$ ($65\ \text{eV}$) and Si ($100\ \text{eV}$) edges precludes accurate background subtraction under the Si $L_{2,3}$ edge; however, semi-quantitative analyses are still possible.

II. RESULTS

A. Differential scanning calorimetry

A representative DSC scan of a multilayer sample is shown in Figure 2, where we plot a difference scan for an intermediate heating rate of 2000 °C/s. The main features of this scan are a relatively large exothermic peak (referred to as peak 1) initiating at a heater voltage (V_h) of 2.55 V (corresponding to 234°C), followed by a smaller exothermic effect (peak 2) starting at 4.28 V (483 °C). We interpret these effects as originating from Ni/Si reactions activated at different temperatures. The later exothermic effect continues beyond the maximum heater voltage into the cooling part of the cycle. These effects are greatly diminished in scans beyond the first, indicating that reaction was nearly complete after the first scan.

In Figure 3, we show a series of 5 DSC scans at different rates. A normalization was used for each scan so that the signals may be conveniently compared, as the raw signal vs. time traces differ significantly both in duration and amplitude. The signal amplitudes for each scan rate were normalized by the respective scan rate, and the abscissa shows time divided by total scan time. This ratio is the fraction of scan completed. Also shown is V_h/V_{hmax} , where V_{hmax} is the maximum heater voltage. The horizontal offset of each DSC scan is adjusted so that all V_h/V_{hmax} plots coincide. Figure 3 shows an interesting evolution in the fine structure of the DSC peaks as the scan rate is increased. At 490 °C/s, peak 1 shows double maxima, the higher voltage (higher temperature) one of which gradually diminishes with increasing scan rate, until no longer distinguishable at 7950 °C/s. As discussed below, this feature may indicate added complexity in the reaction represented by peak 1.

By integrating the areas under the two peaks defined in Figure 2, it is possible to get an estimate of the enthalpy of reaction as a function of scan rate by reference to the Al/Ge eutectic data mentioned above. Results are shown in Figure 4, where the inset indicates the variation of the areas for peak 1 and peak 2 as a function of scan rate. Note that peak 1 decreases from its maximum at the slowest scan rate to nearly zero at the highest scan rate, whereas peak 2 shows the reverse trend. The sums of the two peak areas show a monotonic increase with scan rate, suggesting either that enthalpy production and completion of reaction are enhanced at high scan rates, or that differential heat loss is greater at the slow scan rates. For comparison we also show in Figure 4 the cumulative results of similar experiments on a Ni/Si bilayer. Although the data are less extensive, a similar trend is evident for the bilayer.

B. Post-experimental characterization

In Figs. 5a and 5b we show microstructures of the rapidly scanned vs. slowly scanned multilayered films, as obtained by TEM bright field imaging. A large difference is obvious, in that the rapidly scanned material (5a) is essentially homogeneous, whereas the slow scan (5b) retains a multilayered structure. This is further borne out by the energy-filtered (EFTEM) compositional maps of Figures 5d (Si) and 5e (Ni), which show

a layered heterostructure of alternating Si- and Ni-rich layers. Detailed analysis of the EFTEM spectra for the slow scan showed that substantial interdiffusion of Ni and Si occurred, resulting in relatively homogeneous bilayers of stoichiometrically distinct Ni-silicides. In Figs. 5b and 5c, thin, discontinuous areas with high signal (bright) are evident at every other Ni/Si junction. These small areas have the highest Si concentration and are comprised of a third, Si-rich phase. By contrast with the slowly scanned material of Figure 5b, EFTEM data for the rapidly scanned sample in Figure 5a were featureless and EFTEM (not shown) confirmed no discernible compositional layering; the sample appeared to have become homogeneous with regard to Ni and Si distribution. Due to the partial overlap of Ni and Si edges, quantitative information on phase compositions was not obtained.

Information on identity of crystalline phases in the reacted Ni/Si multilayers was obtained from two sources: 1) selected area electron diffraction (SAD) data taken from FIB samples of the DSC sensors; and 2) x-ray diffraction data on multilayered coupons subjected to a rapid thermal anneal at 50 °C/s. Data from the two sources are consistent in that the principal phases identified are Ni₃Si (major), (Ni,Si) solid solution, NiSi₂ (major) and Si. No measurable difference was observed between the SAD patterns from sections of the slow scanned and the rapidly scanned DSC samples.

IV. DISCUSSION

A. Generalized interpretation

Based on examination of the combined TEM, EFTEM, SAD, XRD and DSC data, we have developed working hypotheses for events occurring during the DSC ramps as follows. As the Ni/Si multilayers were heated, a temperature (~ 235 °C, see Figure 2) was reached where interfacial reaction was initiated, resulting, as the temperature increased further, in the first exothermic energy release, followed by a second energy release peaking near the maximum ramp temperature of 560 °C. As detailed in Figure 4, the intensity of these peaks varied inversely with increasing scan rate, such that the initial peak (peak 1), which was not detectable at the lowest scan rate, became the most intense peak at the highest scan rate. The second peak (peak 2) which was the most intense peak at the slowest scan rate, became undetectable at the highest scan rate. We associate peak 1 with exothermic Ni/Si mixing (rapid diffusion and/or melting) at the thermodynamically unstable Ni/Si interface, and peak 2 with secondary crystallization of Ni silicide phases. The competition between rapid diffusion/melting and crystallization/growth is influenced by the scan rate, such that the rapid process is more pronounced in the rapidly scanned materials, due to kinetic limitations on the crystallization rate of the secondary solid phases. If the rapid mixing process results from melting, it may be to some extent self-sustaining¹⁶ at the highest scan rates where there is less thermal loss, since for the unstable Ni/Si interface, the exothermic energy associated with the negative enthalpy of mixing of Ni and Si greatly exceeds the endothermic effect associated with the disorder of melting. In the most rapidly scanned materials (Figure 5a), complete intermixing of Ni and Si occurred, apparently with nearly simultaneous crystallization, since only one discernible exothermic peak was observed. The

fundamental question relates to the origin of the rapid mixing process: melting vs. rapid diffusion by a short circuit mechanism such as grain boundary diffusion.

B. Metastable melting

The possibility of metastable melting in the rapidly scanned sample can be further evaluated by means of a thermodynamic analysis of the experimental Ni-Si phase diagram. For this purpose, we used Thermocalc¹⁵ for the thermodynamic calculations. The calculations were completed using the thermodynamic descriptions of Tokunaga et al,¹⁷ in which the Gibbs energies of the disordered phases (liquid, f.c.c. Ni solid solution) were modeled as regular solutions with Redlich-Kister interaction parameters fitted to the experimental data. For the ordered f.c.c. Ni phase, an additional contribution to the Gibbs energy associated with ordering was modeled with two sublattices. For the stoichiometric phases appearing in the Ni-Si phase diagram (including Ni₃Si and NiSi₂), Gibbs energies were calculated from the weighted energies of the pure end members combined with an empirical term to fit the experimental data. The resulting equations of state allowed the calculation of metastable equilibria among any combination of Ni-Si phases over a wide range of temperatures.

In Figure 6a, the complete Ni-Si diagram calculated with the optimized parameters of Tokunaga et al¹⁷ is presented; the diagram contains 11 distinct phases. In Figure 6b we show the results of calculating metastable equilibria among just three of the phases: the pure Ni and Si end members, and the liquid phase. This scenario corresponds to the situation of ultra rapid heating where there is no time for growth of intermediate crystalline phases, only formation of a melt. The phase diagram of Figure 6b indicates a deep trough of metastable liquid extending to low temperatures, and centered at approximate composition 0.33 mole fraction Si. This metastable liquid encompasses (fortuitously) the bulk composition chosen for the multilayer films (0.35 mole fraction Si), giving credence to the possibility of extensive metastable melting for the rapidly heated multilayers. In Figure 6c we have calculated metastable equilibria with one additional phase, the ordered f.c.c. solid solution. The presence of the ordered solid solution phase significantly reduces the region available for metastable melting and the minimum melting temperature is raised to 400 °C.

C. Solid state diffusion

If only solid state diffusion is considered without melting, the complete homogenization of the rapidly heated multilayers relative to the remnant layering of the slowly heated samples is counterintuitive. Nonetheless, it is useful to consider diffusion from a more quantitative perspective. Assuming a composition-independent diffusivity, the Fickian diffusion formalism

$$\frac{\partial C}{\partial t} = D \frac{\partial^2 C}{\partial x^2}$$

where C = concentration of Ni, x = distance, and t = time, with boundary conditions

$$x = 0 \text{ and } x = L : \frac{\partial C}{\partial x} = 0$$

and initial conditions

$$t = 0 : C = kC_0$$

where

$$k = 0 \ (x < L/2), \ k = 1 \ (x \geq L/2)$$

can be solved numerically using an error function solution to give concentration profiles approximating the expected Ni and Si distribution at 560 °C as a function of time. For these calculations we have assumed that the Ni diffusion relative to Si is the more rapid process. Since the sputtered films are granular, we have also assumed that grain boundary diffusion is the dominant mass transport mechanism. During reactive diffusion, the diffusivities of Ni through the product phases must be considered. Literature data are few, but representative grain boundary diffusivity ($D(\text{gb})$) values in different matrices are summarized in Table 1, where it can be seen that values vary widely.

Specifically, the difference between Ni transport in NiSi_2 vs. Ni_2Si is about six orders of magnitude, which would have an extreme effect on the calculated concentration profiles at the Ni/Si interface. In Figure 7, we show a diffusion profile calculated with $D(\text{gb})$ for Ni/ NiSi_2 . The Ni mass transport is represented in the figure by C/C_0 , the ratio of the Ni concentration after a scan to the concentration before the scan shown as a function of the distance from the interface. The calculation shown by the solid line in Figure 7 corresponds to the approximate time at 560 °C which would result from a 16,000 °C/s scan. For this situation, the diffusion is limited to a region of less than 2 nm at the interface. The dashed line in Figure 7 shows a profile calculated for a 120 °C/s scan, where the predicted mass transport is similar to that observed in Figure 5b. Significant transport of Ni has occurred throughout the 20 nm extent depicted in the model, yet homogenization has not occurred. If the $D(\text{gb})$ value for Ni in Ni_2Si or the generalized value for Ni diffusivity in a metal matrix are used, essentially complete homogenization results for both scan rates. Thus, different diffusivities are required to explain the results of slow vs. rapid scan rates. This suggests an active role of NiSi_2 at the slow scan rates and increased influence of other phases such as metastable liquid or glass, or Ni-rich silicides (e.g. Ni_3Si) with higher diffusivities at the rapid scan rates. We know from SAD and XRD that NiSi_2 and Ni_3Si are major product phases for both scan rates. The compositional layering evident in Figures 5d,e could be explained by the influence of an NiSi_2 -rich layer, which would serve as an effective diffusion barrier, preventing further homogenization in the slow scans. The lack of layering in Figure 5a, together with the diffraction data implies interspersed Ni_3Si and NiSi_2 in the rapid scan products. It seems unlikely on microstructural grounds that a completely interspersed, relatively uniform texture would result from interfacial mass transport in the solid state, since there has to be a continuous directional component to the mass flux and associated reaction. An efficient homogenization process seems to be required, for which melting provides the most probable explanation.

D. Effect of scan rate on reaction energetics

It is useful to compare the observed enthalpies (Figure 4) with the values computed²¹ for complete reaction to Ni_2Si and NiSi (the equilibrium products predicted

by Figure 6a for 0.35 mole fraction Si) versus reaction to the observed products (Ni_3Si and NiSi_2). Our calculations suggest 8.9 μJ for the equilibrium reaction and 8.3 μJ for our observed products. The maximum value observed at the most rapid scan rates in Figure 4, i.e. 9.8 μJ , is higher than the maximum predicted for the equilibrium phase assemblage. We attribute this to added energies associated with the amorphous to crystalline transition in Si, and to spontaneous grain growth in Ni. With these caveats, the DSC data appear to be in reasonable agreement (within 15%) of predicted values.

The fine structure of peak 1 revealed in Figure 3 suggests the need for further interpretation. For example, it is possible that a small amount of melting (the first maximum of the doublet of peak 1) occurs even in the slow scans, but that this melting gives way to crystallization (e.g. NiSi_2) (the second maximum of the doublet), that impedes further melting and homogenization. As the scan rate increases, the time available for NiSi_2 to form is less, so that the amount of melting increases, resulting in a diminished doublet. At the highest scan rate, melting and complete homogenization occur simultaneously with the crystallization of Ni_3Si and NiSi_2 products, resulting in a combination of peaks 1 and 2.

V. CONCLUSIONS

In summary, we favor the application of a metastable melting hypothesis to explain the enhanced mass transport and microstructure produced by the ultra-rapid heating of the Ni/Si multilayers (DSC scan rate 16,000 $^\circ\text{C}/\text{s}$), whereas we postulate that solid state diffusion is responsible for the microstructure produced by the slow scan rate (120 $^\circ\text{C}/\text{s}$). Our observations and conclusions regarding the reactions to form the silicide phases Ni_3Si and NiSi_2 as final reaction products appear to be consistent with the DSC enthalpies, and the relatively low grain boundary diffusivity of NiSi_2 . These results point to the possibility of alternative routes for practical processing of semiconductor silicide interconnects under conditions of flash annealing. Further combined microstructural/nano-DSC experiments will provide more details on the potential use of ultra-rapid-heating in Si-based device fabrication.

¹ Semiconductor Industry Association, International Technology Roadmap for Semiconductors: Semiconductors 2007 Edition Front End Processes p 29-30; 181 Metro Drive, Suite 450 San Jose, CA 95110, <http://public.itrs.net>.

² E. P. Gusev, V. Narayanan, M. M. Frank, IBM J. Res. & Dev. **50**, 387 (2006)

³ W.J. Lee, D.W. Kim, S. Y. Oh, Y. J. Kim, Y. Y. Zhang, Z. Zhong, S. G. Li, S. Y. Jung, I. S. Han, T. K. Gu T. S. Bae, G. W. Lee, J. S. Wang, and H.D. Lee J. Appl. Phys. **101**, 103710 (2007)

⁴ N. Biswas, J. Gurganus, and V. Misra, Appl. Phys. Lett. **87**, 171908 (2005);

- ⁵ C. Rivero, P. Gergaud, M. Gailhanou, and O. Thomas, B. Froment, H. Jaouen, and V. Carron, *Appl. Phys. Lett.* **87**, 041904 (2005);
- ⁶ J. A. Kittl, M. A. Pawlak, C. Torregiani, A. Lauwers, C. Demeurisse, C. Vrancken, P. P. Absil, and S. Biesemans, *Appl. Phys. Lett.* **91**, 172108 (2007)
- ⁷ R. Lindsay, B. Pawlak, J. Kittl, K. Henson, C. Torregiani, S. Giangrandi, R. Surdeanu, W. Vandervorst, A. Mayur, J. Ross, S. McCoy, J. Gelpey, K. Elliott, X. Pages, A. Satta, A. Lauwers, P. Stolk, and K. Maex, *Mat. Res. Soc. Symp. Proc.* **765**, paper number D7.4.1 (2003)
- ⁸ W. Skorupa, W. Anwanda, D. Panknina, M. Voelskowa, R.A. Yankova and T. Gebel, *Vacuum* **78**, 673 (2005)
- ⁹ B. Adams, D. Jennings, K. Ma, A. J. Mayur, S. Moffatt, S. G. Nagy, V. Parihar, *Proceedings of the 15th IEEE International Conference on Advanced Thermal Processing of Semiconductors - RTP2007*, Catania, Italy, 155-160 (2007).
- ¹⁰ Y. Setiawan, P. S. Lee, and K. L. Pey, *Appl. Phys. Lett.* **88**, 113108 (2006)
- ¹¹ S.E. Thompson, S Parthasarathy, *Materials Today* **9**, 20 (2006)
- ¹² F. Nemouchi, D. Mangelinck, C. Bergman, and P. Gas, *Appl. Phys. Lett.* **86**, 041903 (2005).
- ¹³ L. A. Clevenger, C. V. Thompson, R. C. Cammarata, and K. N. Tu, *Appl. Phys. Lett.* **52**, 795 (1988)
- ¹⁴ R. E. Cavicchi, G. E. Poirier, N. H. Tea, M. Alfridi, D. Berning, A. Hefner, J. Suehle, M. Gaitan, S. Semancik, and C. Montgomery, *Sensors and Actuators B: Chemical* **97**, 22 (2004).
- ¹⁵ Certain commercial equipment, instruments, or materials are identified in this document. Such identification does not imply recommendation or endorsement by the National Institute of Standards and Technology, nor does it imply that the products identified are necessarily the best available for the purpose.
- ¹⁶ L. A. Clevenger, C. V. Thompson, and K. N. Tu, *J. Appl. Phys.* **67**, 2898 (1990)
- ¹⁷ T. Tokunaga, K. Nishio, H. Ohtani, and M. Hasebe, *CALPHAD* **27**, 161 (2003).

- ¹⁸ C. Hayzelden and J. L. Batstone, *J. Appl. Phys.* **73**, 8279 (1993)
- ¹⁹ W. Losch and W. Acchar, *Physica Status Solidi (a)* **173**, 275 (1999)
- ²⁰ A. M. Brown and M. F. Ashby, *Acta Met.* **28**, 1085 (1980)
- ²¹ C. W. Bale, P. Chartrand, S.A. Degterov, G. Eriksson, K. Hack, R. Ben Mahfoud, J. Melancon, A. G. Pelton, and S. Peterson, *CALPHAD* **26**, 189 (2002).

Table 1. Relevant diffusivities at 560 °C

<u>Species / Matrix</u>	<u>D(gb)(m²/s)</u>	<u>Reference</u>
Ni / NiSi ₂	3.9 x 10 ⁻¹⁸	18
Ni / Ni ₂ Si	~5 x 10 ⁻¹²	19
Ni / metal (avg.)	5 x 10 ⁻¹⁴	20

Figure Captions

Figure 1. Photomicrograph and schematic of nanocalorimeter.

Figure 2. DSC signal and heater voltage vs. time for 2000 °C/s ramp rate for the multilayer sample.

Figure 3. DSC signal divided by the scan rate for 5 scan rates plotted against normalized scan time. Also shown is the normalized applied heater voltage V_h .

Figure 4. Sum of peak area (enthalpy) vs scan rate for multilayer (circles) and bilayer (solid triangles). Inset: peak 1 enthalpy (diamonds), peak 2 enthalpy (squares), and sum of peak areas (circles) vs. scan rate for multilayer sample.

Figure 5. Transmission electron microscopy images from Ni/Si multilayer sample annealed with a ramp rate of (a) 16,000 °C/s and (b-e) 120 °C/s. (c) Magnified brightfield image. (d, e) EFTEM maps for Si and Ni from the same area.

Figure 6. (a) Calculated Ni-Si equilibrium phase diagram; (b) diagram assuming metastable equilibria among the pure Ni and Si end members and the liquid phase; (c) metastable equilibria among Ni solid solution, Si, ordered f.c.c. phase, and liquid; (d) metastable equilibria among pure Ni and Si end members, Ni_3Si , $NiSi_2$, and liquid.

Figure 7. Diffusion profile calculated with $D(gb)$ for Ni/ $NiSi_2$. Solid line represents calculation for a 16,000 °C/s scan, and dashed line is for a 120 °C/s scan. C/C_0 is the ratio of the Ni concentration after a temperature scan to the concentration before the scan.

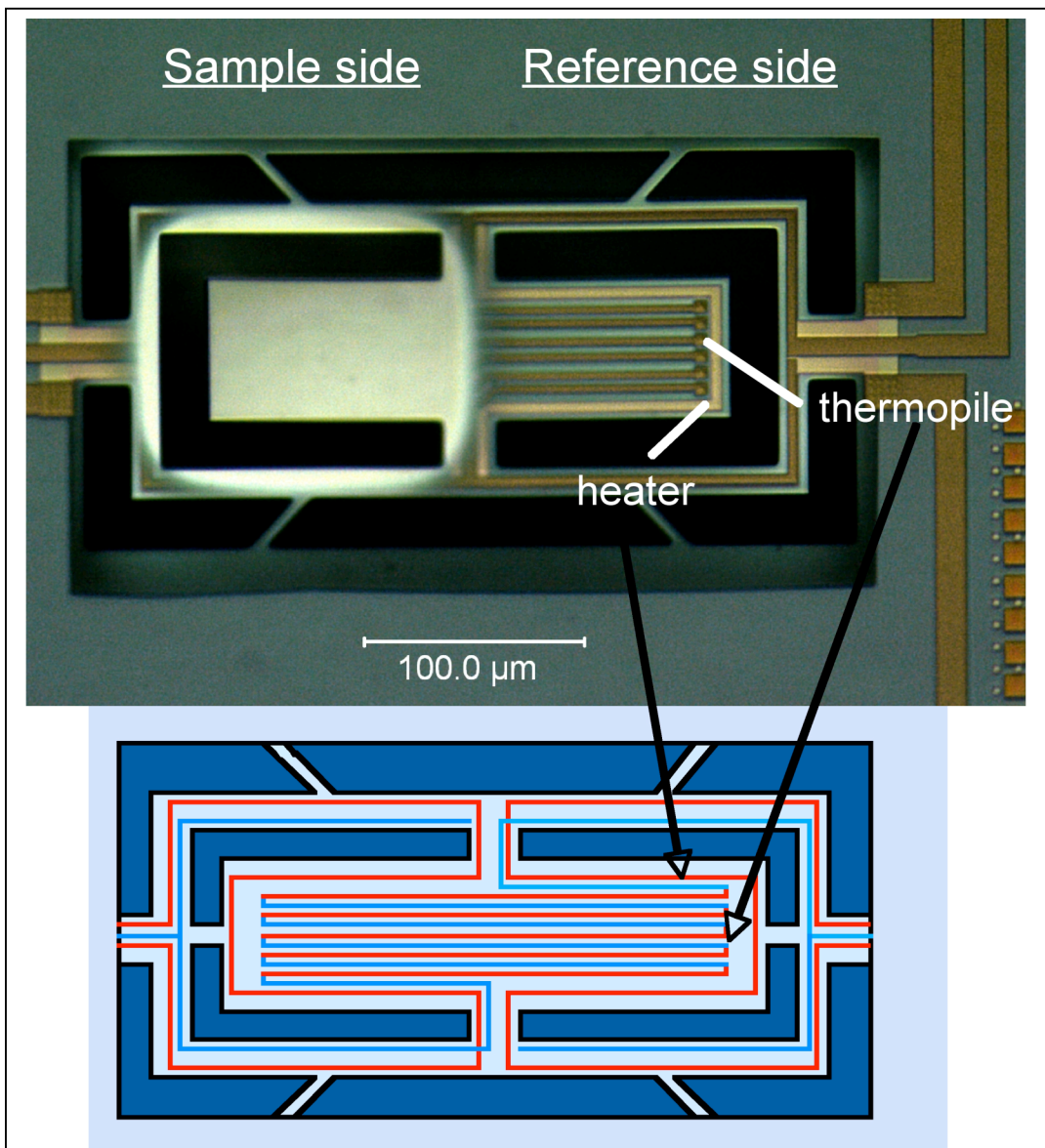


Figure 1. Photomicrograph and schematic of nanocalorimeter.

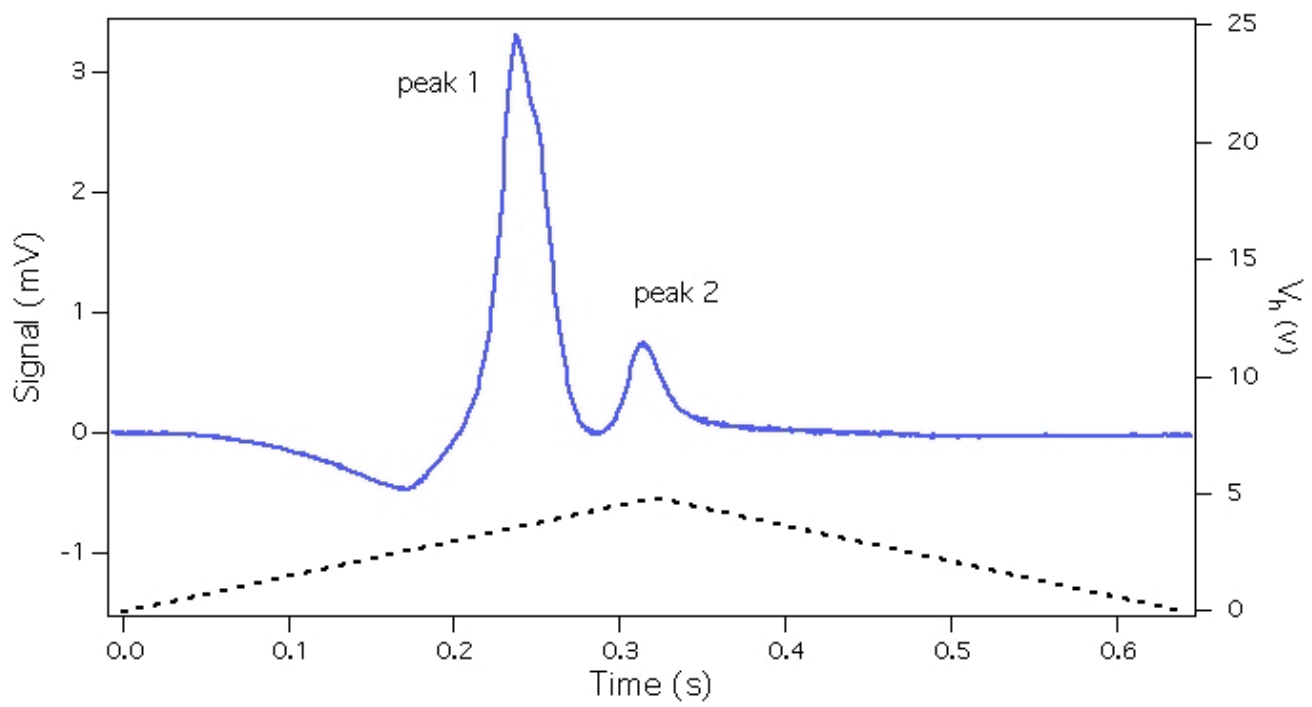


Figure 2. DSC signal and heater voltage vs. time for 2000 °C/s ramp rate for the multilayer sample.

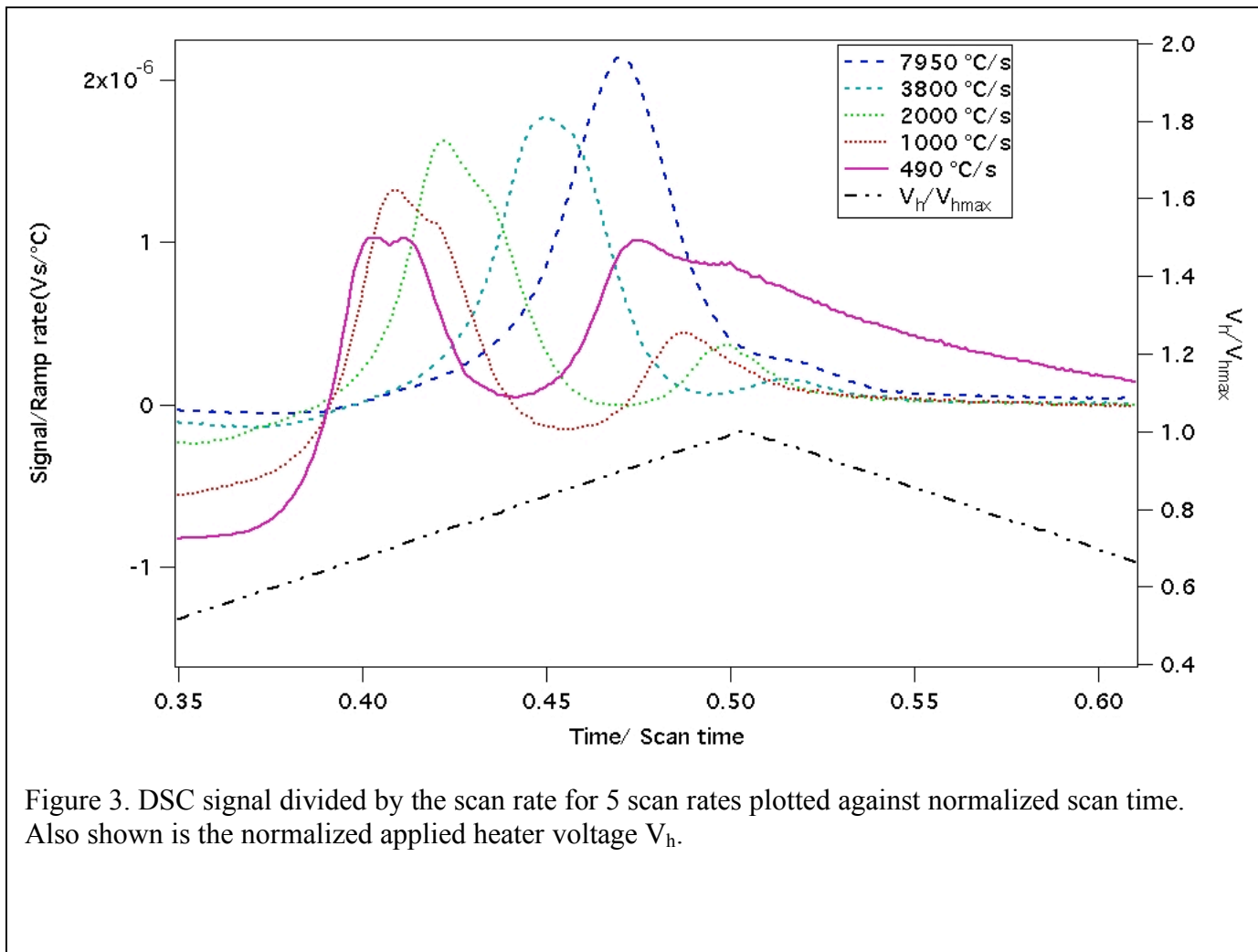


Figure 3. DSC signal divided by the scan rate for 5 scan rates plotted against normalized scan time. Also shown is the normalized applied heater voltage V_h .

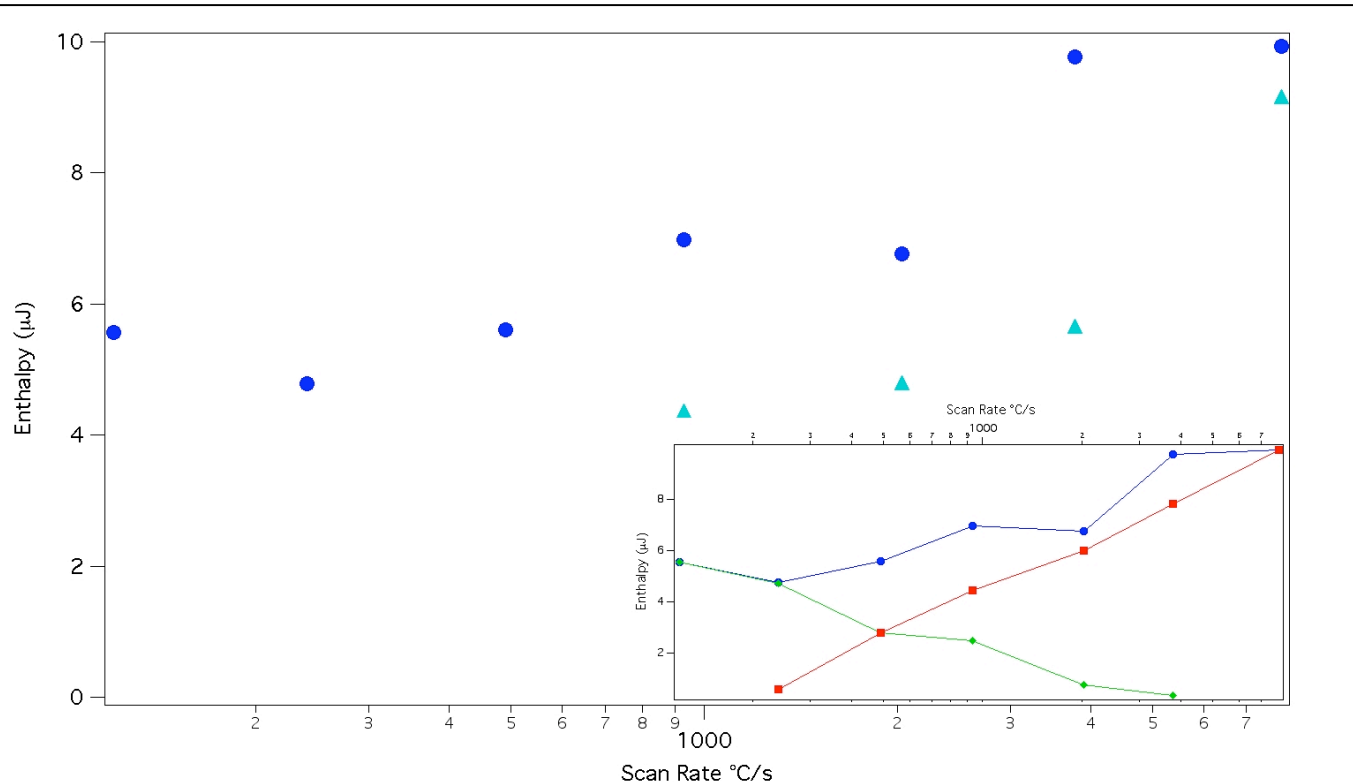


Figure 4. Sum of peak area (enthalpy) vs scan rate for multilayer (circles) and bilayer (solid triangles). Inset: peak 1 enthalpy (diamonds), peak 2 enthalpy (squares), and sum of peak areas (circles) vs. scan rate for multilayer sample.

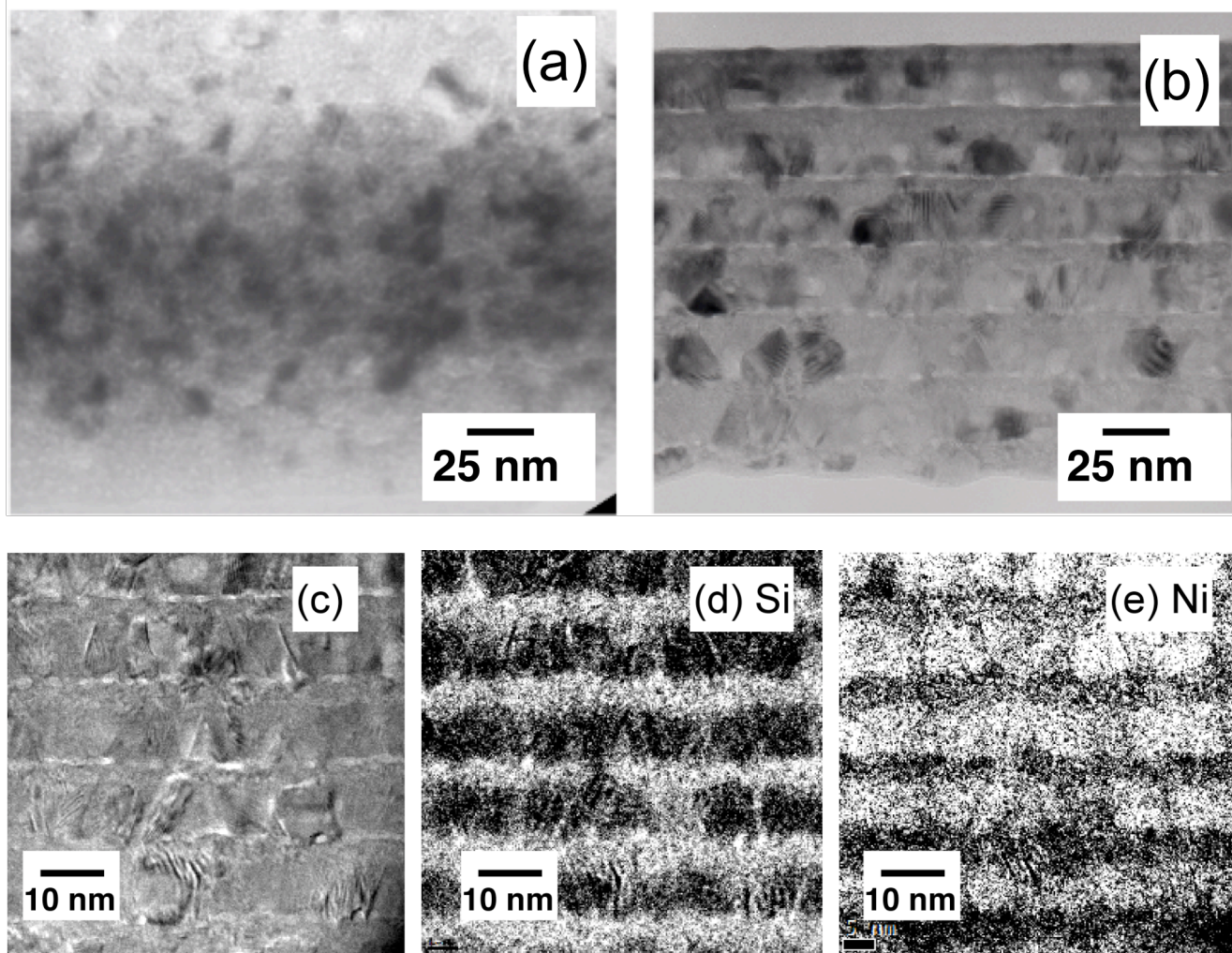


Figure 5. Transmission electron microscopy images from Ni/Si multilayer sample annealed with a ramp rate of (a) 16,000 °C/s and (b-e) 120 °C/s. (c) Magnified brightfield image. (d, e) EFTEM maps for Si and Ni from the same area.

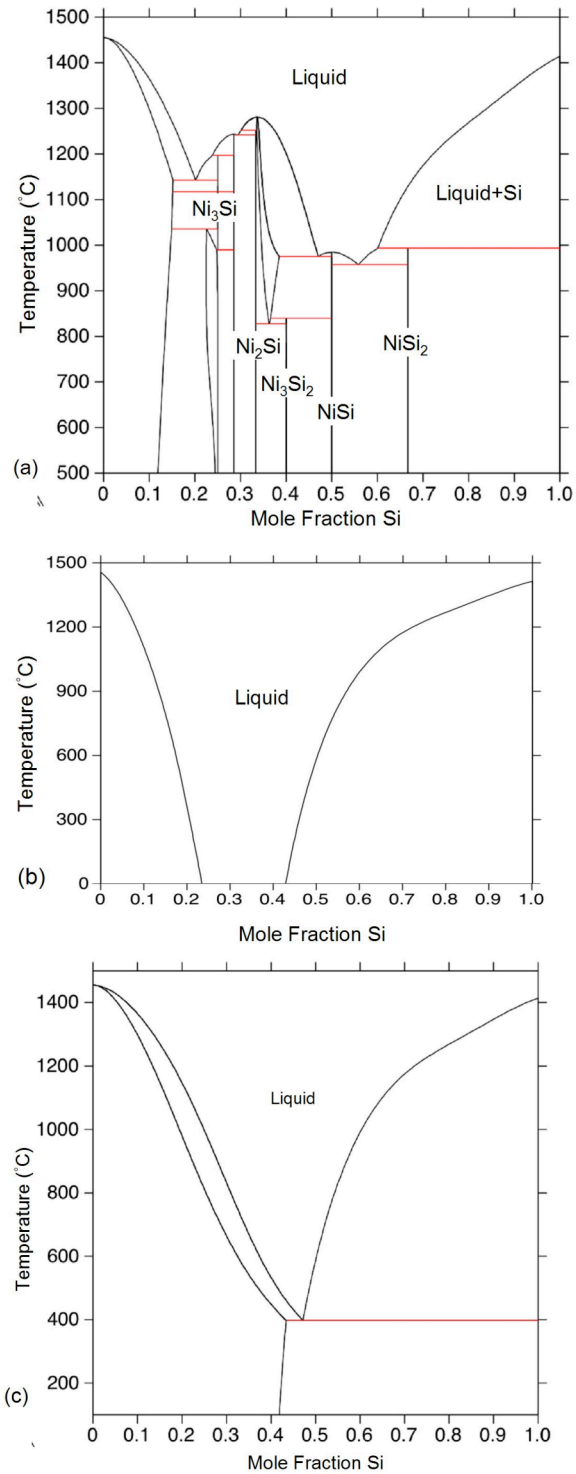


Figure 6. (a) Calculated Ni-Si equilibrium phase diagram; (b) diagram assuming metastable equilibria among the pure Ni and Si end members and the liquid phase; (c) metastable equilibria among pure Ni and Si end members, ordered f.c.c. phase, and liquid.

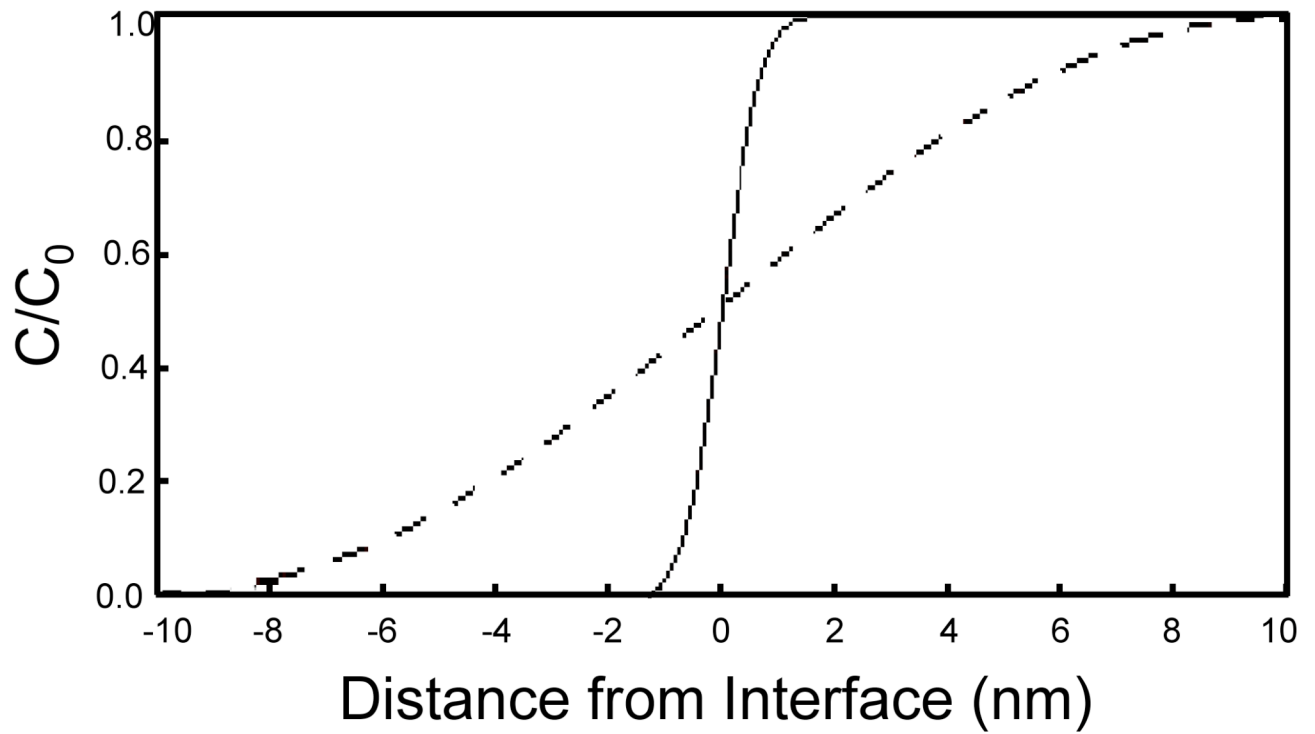


Figure 7. Diffusion profile calculated with $D(\text{gb})$ for Ni/NiSi₂. Solid line represents calculation for a 16,000 °C/s scan, and dashed line is for a 120 °C/s scan. C/C_0 is the ratio of the Ni concentration after a temperature scan to the concentration before the scan.